Digest Journal of Nanomaterials and Biostructures Vol. 20, No. 4, October-December 2025, p. 1587-1598

The influence of TiO_2 coating on the coloring and NIR properties of yellow pigments

J. H. Lu [a], Q. Shen [b], M. H. Xu [b, *], J. R. Chu [a], X. Ling [a]
[a] *Zhejiang Zhongyi Construction Group Co., Ltd.*
[b] *Department of Materials Engineering, Huzhou University, Huzhou 313000, China*

In this paper, TiO_2 was coated on yellow pigment (FeOOH) to prepare coated pigment (FT*x*). The test results from X-Ray Diffraction (XRD), Scanning Electron Microscope (SEM), transmission electron microscopy (TEM) and (Kelvin probe force microscopy) KPFM show that the surface of FeOOH has been coated with TiO_2. It is noteworthy that there is electron transfer between pigment interfaces. In addition, the amount of TiO_2 has a significant impact on the coloration of FeOOH and its near-infrared reflectance (NIR). The NIR of FT_{16} (L^* = 84.75, a* = 7.5, b^* = 25.13) reaches 81.37%, much higher than the 61.07% of FeOOH pigment (L^* = 70.33, a^* = 12.91, b^* = 33.87). The TiO_2 coating amount shows exponential correlations with both chromaticity parameters and reflectance, while a strong linear relationship exists between NIR and L^*. The application of TiO_2 coating improves the pigment's brightness and its reflectivity in the near-infrared range, suggesting its potential as a functional cooling pigment for radiative control applications.

(Received October 10, 2025; Accepted December 16, 2025)

Keywords: Iron oxide yellow pigment, Cold pigment, Coated, TiO_2, NIR

1. Introduction

Solar radiation provides essential energy to Earth, yet it can also lead to undesirable surface heating of objects. In sectors such as construction, petroleum, and transportation, excessive surface temperatures are problematic as they necessitate increased reliance on cooling systems, thereby raising energy consumption and refrigeration costs [1,2]. As a result, countries are actively conducting research on infrared thermal reflective coatings and pigments that mainly reflect near-infrared radiation in sunlight. These pigments, when applied to material surfaces, can reflect invisible yet energy-rich near-infrared radiation, helping to lower internal temperatures, preserve chemical stability under heat, and offer a range of color options [3,4]. Their use can significantly cut down on cooling system usage, contributing to energy conservation and cost reduction in manufacturing.

The thermal reflective performance of pigments is closely tied to its color. Among all pigments, white pigment exhibits the highest solar reflectivity [5]. For example, titanium dioxide (TiO_2) has a solar reflectance of approximately 87% and is frequently employed as a cooling pigment [6]. Rutile TiO_2, one of the earliest inorganic pigments used in thermal insulation coatings, demonstrates over 85% reflectance in the near-infrared range and nearly 100% reflectance in the visible spectrum [7]. However, the aesthetic appeal of purely white surfaces is limited, prompting the need for colored alternatives.

Yellow pigments, known for their vibrant hues and versatile properties, are found in extensive use across various industries. Common types include titanium nickel yellow and titanium chromium yellow, which are applied in engineering plastics and automotive coatings, as well as iron oxide yellow, commonly used in architectural and decorative applications. Researchers worldwide are actively developing novel yellow pigments designed for effective solar radiation management.

* Corresponding authors: xumh123@163.com
https://doi.org/10.15251/DJNB.2025.204.1587

For instance, L. Li et al. synthesized a yellow pigment, $(Li_{0.4}La_{0.6}Al_{0.6})_{0.1}Bi_{0.8}][Mo_{0.2}V_{0.8}]O_4$ (b^* = 77.13, C^* = 77.6), through calcination at 700 °C [8]. X. He et al. developed a core-shell structure $NiTiO_3$@TiO_2 yellow pigment by calcining a precursor formed via Ni^{2+} precipitation on TiO_2 particle surfaces, which enhanced near-infrared reflectivity (NIR) [9]. J. Zou et al. produced Ni-doped $BaTi_5O_{11}$ yellow pigment using a solid-state method at 1000 °C for 2 h, achieving a near-infrared reflectance of 76.9% [10]. TiO_2@$NiTiO_3$ composite pigments were also synthesized via a precipitation-calcination process, the yellow intensity (b^*) increased with larger microcrystalline sizes [11]. However, most of these methods rely on high-temperature solid-state synthesis, which is energy-intensive.

Iron oxide yellow pigment, also referred to as hydrated iron oxide, has the chemical formula $Fe_2O_3 \cdot H_2O$ or α-FeOOH. Its hue ranges from lemon yellow to orange, depending on crystal size, with typical particle sizes between 0.5 to 2 μm. This pigment offers excellent lightfastness, weather resistance, and alkali resistance, making it widely used in coatings, construction materials, plastics, and rubber [12,13]. As a traditional pigment, in order to improve its market competitiveness, there is an urgent need to explore new functional applications.

In this study, TiO_2 was coated onto inorganic iron oxide yellow pigments to enhance their optical properties by improving light reflection, refraction, or scattering, thereby increasing their NIR. The structural characteristics and NIR of the prepared pigments were analyzed using SEM and UV-Vis-NIR spectroscopy. The effect of TiO_2 coating on pigment coloring and reflective properties has also been studied. The prepared yellow pigments demonstrate the ability to effectively reflect high-energy near-infrared radiation from sunlight, reducing surface heat absorption and lowering object surface temperatures, thus contributing to energy efficiency and reducing carbon emissions. The prepared yellow pigment can also be applied in fields such as construction, transportation, industrial production, etc.

2. Experimental section

2.1 Materials

Yellow pigments (FeOOH), were provided by Zhejiang Huayuan Pigments Co., Ltd. The anhydrous ethanol, tetra-n-butyl titanate and other reagents were provided by Macklin Reagent (Shanghai) Co., Ltd. Distilled water was used as a solvent during the experiment.

2.2 Preparation of coated pigments

2.2.1 Coating pigment with varying amounts of TiO_2

To investigate the effect of different coating thicknesses, TiO_2-coated pigments were synthesized using varying quantities of butyl titanate. In a typical process, FeOOH (0.5 g) was placed in a conical flask, then anhydrous ethanol (50 mL). The suspension was magnetically stirred at 40 °C for 0.5 h to form a uniform dispersion. Next, tetra-n-butyl titanate (2 mL) was introduced, and the mixture was continuously stirred (2 h). Afterwards, H_2O (16 mL) and ethanol (24 mL) were added, and the solution was stirred for 2 h. The resulting sample was collected via suction filtration, thoroughly rinsed with distilled water, and dried at 60 °C for 8 h, yielding the coated pigment labeled FT_2. By repeating the same procedure with 4 mL, 8 mL, 12 mL, and 16 mL of butyl titanate, respectively, the samples FT_4, FT_8, FT_{12}, and FT_{16} were obtained.

2.2.2 Synthesis of coated pigments under varied solvent ratios

In another set of experiments, the influence of solvent composition on the coating process was examined. FeOOH (0.5 g) was placed into a conical flask with 50 mL of absolute ethanol. The mixture was stirred magnetically in a water bath (40 °C) for 30 min to get a stable dispersion. Subsequently, 4 mL of butyl titanate was added, and then the solution was stirred for 2 h. Then, a mixture of 4 mL water and 6 mL ethanol was added, and the reaction continued for another 2 h under continuous stirring. The final product was filtered, dried, and designated as FT-4DW. The same procedure was repeated using different solvent ratios: 8 mL water + 12 mL ethanol (FT-8DW), 12 mL water + 18 mL ethanol (FT-12DW), 16 mL water + 24 mL ethanol (FT-16DW), and 20 mL water + 30 mL ethanol (FT-20DW).

2.3.3 Effect of different reaction times

To evaluate the impact of reaction time on the coating process, coated pigments were prepared under varying time conditions. Briefly, 0.5 g of FeOOH and 50 mL of ethanol were placed in a conical flask. Magnetic stirring was carried out for 30 min at 40 °C. Then, 4 mL of butyl titanate was added, and the mixture was stirred for 2 h. Following this, H_2O (16 mL) and ethanol (24 mL) were introduced, and the reaction was stirred for a second time (1 h). The resulting product was filtered and dried to obtain the sample labeled FT-1h. The same procedure was repeated, adjusting the second stirring duration to 1.5 h, 2 h, 2.5 h, and 3 h, resulting in the samples FT-1.5h, FT-2h, FT-2.5h, and FT-3h, respectively.

2.3 Characterization

X-ray diffraction patterns were obtained using a X-ray diffractometer (Bruker, D8 ADVANCE) operating at 40 kV and 25 mA. The surface morphology of pigments was examined using a scanning electron microscope (Zeiss Sigma 300) at an accelerating voltage of 15 kV. Using an electron microscope (FEI Tecnai F20) to obtain transmission electron microscopy (TEM) images. Conduct atomic force microscopy (AFM) and Kelvin probe force microscopy (KPFM) measurements using the Bruker Dimension Icon system. During testing, current is applied to the probe with a gold probe as a tip. The potential and work function of the gold probe in this test are −86.3 mV and 5.2 eV, respectively. The optical properties, including ultraviolet-visible and near-infrared reflectance, were analyzed using a UV-Vis-NIR spectrophotometer (Perkin Elmer, Lambda 1050+). Near-infrared reflectance (700–2500 nm), along with color parameters such as *L*, a*, b** were calculated following the procedures outlined in references [5,14].

3 Results and Discussion

3.1 Morphological analysis

The SEM images of FeOOH show a typical needle-like morphology (Fig.1a), with lengths ranging from approximately 0.5 to 1.5 μm and widths between 100 nm and 150 nm. Some minor particle agglomeration is observed, which aligns with the expected structural features of α-FeOOH. Upon coating FeOOH with TiO_2 (Fig.1b), a noticeable transformation in morphology occurs. An obvious coating layer forms around the rod-like FeOOH particles, resulting in an increased width of approximately 200 to 400 nm. Following the TiO_2 coating process, the FeOOH develops a compact layer composed of fine particles on its surface (Fig.1c and 1d), with a thickness of about 40 to 75 nm, altering the original needle-like morphology of FeOOH. The EDS spectrum (Fig.1e) confirms the presence of Fe, O, and Ti elements in FT_8, consistent with its expected composition. Additionally, the EDS elemental mapping in Fig. 1f illustrates a uniform distribution of O, Fe, and Ti throughout FT_8. These morphological observations confirm that the surface coating of FeOOH is successful.

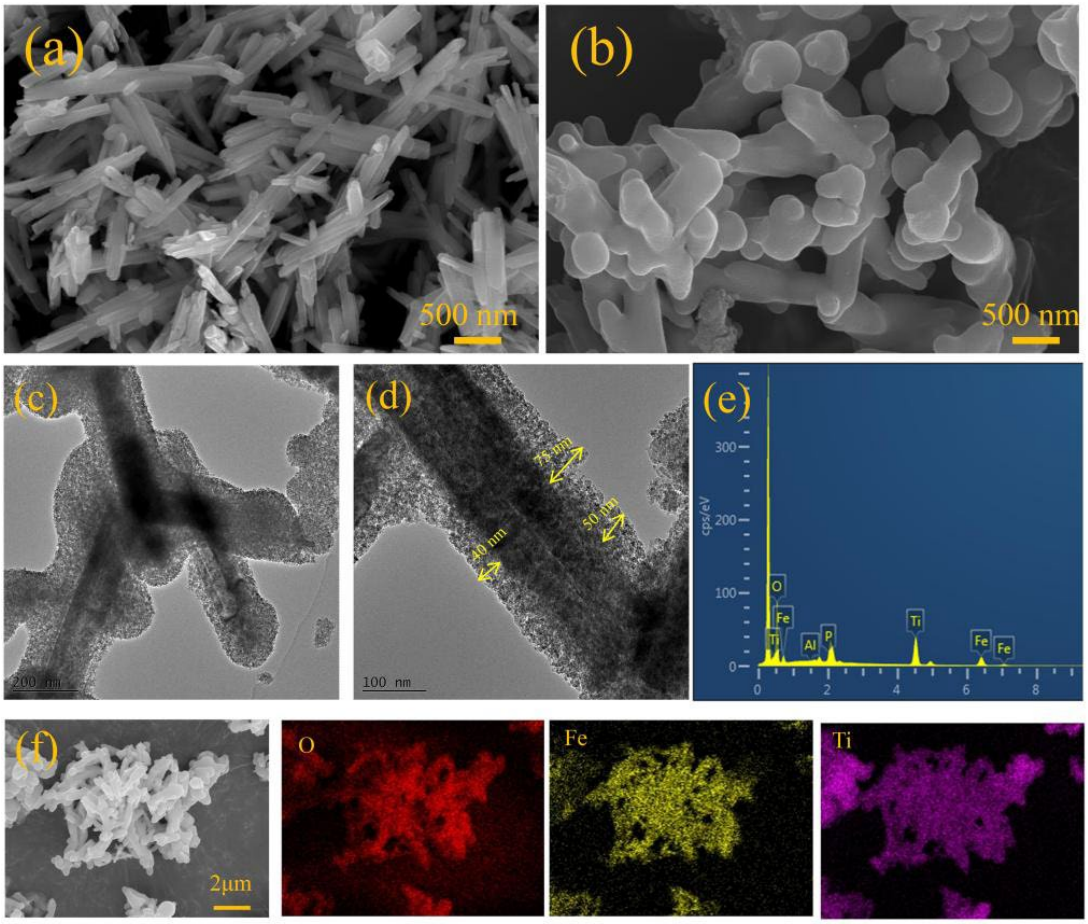

Fig. 1. SEM image of (a) FeOOH and (b) FT_8, TEM images of FT_8 (c,d), EDS spectrum of FT_8 (e), and elemental mapping of FT_8 (f).

3.2 Work function test

To investigate charge transfer behavior within the synthesized pigments, KPFM was employed to measure surface potential variations. KPFM operates by detecting the contact potential difference (CPD) between the probe tip and the surface of pigments, as detailed in references [15,16]. Fig.2 presents the surface potential distribution of pigments. From the same figure, the root mean square roughness (*Rq*) of each sample was derived. FeOOH exhibits an *Rq* value of 51.4 nm, TiO_2 shows 3.36 nm, and FT_8 has a significantly higher *Rq* of 277 nm. This notable difference in surface roughness supports the successful deposition of TiO_2 onto FeOOH.

The KPFM results and related calculations summarized in Table 1 reveal variations in CPD, work function (*W*), and Fermi level (E_f) among FeOOH, TiO_2, and FT_8. Upon coating FeOOH with TiO_2 to form FT_8, electrons migrate from TiO_2 (E_f = -4.10 eV) to FeOOH (E_f = 4.20 eV) until the Fermi levels reach equilibrium at the interface. This indicates the occurrence of interfacial electron transfer within the pigment structure [17].

Table 1. The work function and E_f values of pigments.

Sample	Tested contact potential difference /mV	Work functions (W) /eV	E_f /eV
FeOOH	913	4.20	-4.20
TiO_2	1010	4.10	-4.10
FT_8	967	4.15	-4.15

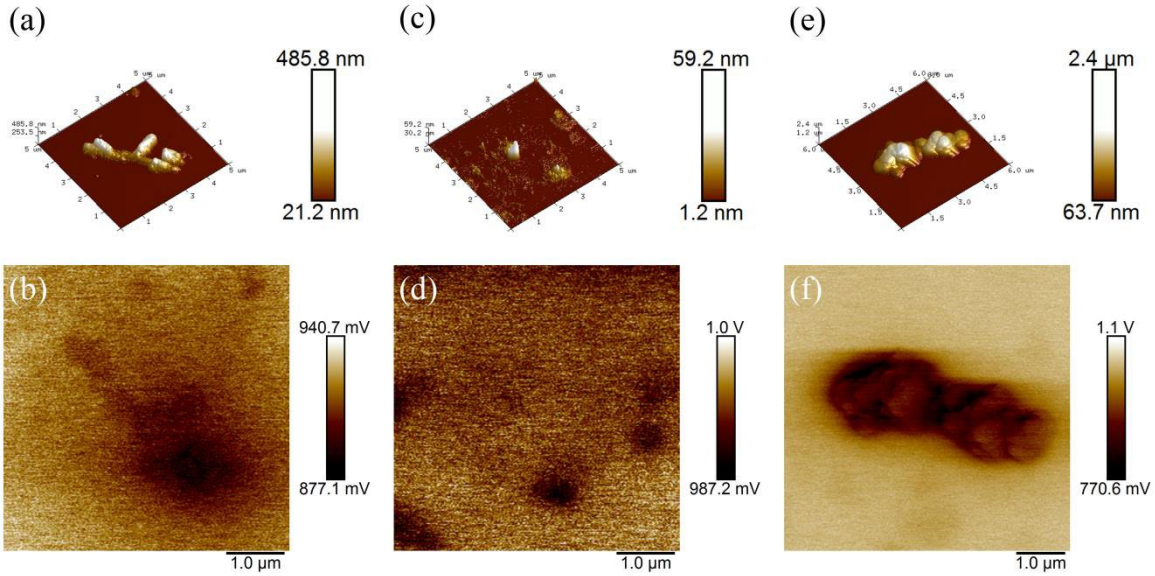

Fig. 2. AFM and KPFM images of pigments. FeOOH (a, b), TiO_2 (c, b) and FT_8 (e, f).

3.3 The influence of TiO_2 dosage

To evaluate how the TiO_2 dosage affects the crystal structure of coated pigments, XRD patterns of prepared pigments were analyzed, as shown in Fig. 3. In Fig.3a, the diffraction peaks of FeOOH at 2θ about 17.8°, 21.2°, 34.7°, 35.5°, 36.6°, 53.1°, and 59.0° correspond to the crystal planes (020), (110), (021), (111), (221), and (151), respectively. These peaks conform to the characteristic structure of FeOOH (JCPDS No. 29-0713) [15]. Under identical synthesis conditions, when TiO_2 was prepared without the presence of FeOOH, a broad diffraction peak appears near 26° (2θ), suggesting that the produced TiO_2 is amorphous. However, when TiO_2 is applied as a coating on FeOOH to form FT_8, the XRD pattern reveals that the structure of FeOOH remained unchanged, while a diffraction peak corresponding to TiO_2 emerged at approximately 2θ = 26°, indicating that FT_8 retains the structural features of both FeOOH and TiO_2.

As the TiO_2 coating dosage increases (Fig.3b), the diffraction peaks associated with FeOOH remain largely unchanged, that is the coating process does not alter the crystalline structure of FeOOH. But, a broad peak near 26° (2θ) becomes more pronounced with increasing TiO_2 dosage, likely due to the thickening of the TiO_2 layer, which enhances the detectability of its diffraction signal.

Fig. 3c and 3d illustrate the impact of TiO_2 dosage on the color and chromatic characteristics of coated pigment. Visual inspection of the pigments reveals that as the TiO_2 coating increases, the yellow hue becomes progressively lighter. As shown in Fig. 3d, the chromaticity coordinates of the coated pigment shift toward the yellow-green region with higher TiO_2 loading. In Table 2, the color parameters indicate that the value of brightness (L^*) increases gradually, while both the a^* and b^*

values decrease. This trend can be attributed to the white nature of TiO_2, which enhances the brightness (L^*) of the pigment while simultaneously diluting the red-green (a^*) and yellow-blue (b^*) color components of original pigment.

Fig. 3e presents the influence of TiO_2 dosage on the reflectance properties of coated pigment. It is evident that increasing the TiO_2 coating leads to higher total solar reflectivity (TSR) and NIR of the pigment. It is worth noting that as summarized in Table 2, FT_{16} exhibits the highest TSR of 70.1% and NIR of 81.37%. This improvement is attributed to the white TiO_2 coating, which effectively reflects sunlight, particularly in the 500–1000 nm wavelength range, thereby enhancing both values of TSR and NIR.

Fig. 3f displays the solar radiation energy distribution of the prepared pigments based on the ASTM standard, primarily concentrated within the 500–1300 nm range. The TiO_2-coated pigments demonstrate enhanced solar shielding performance. Because of their high NIR, these pigments reflect a greater portion of incident solar radiation, reducing the amount of heat absorbed by building surfaces and thus contributing to lower solar heat gain.

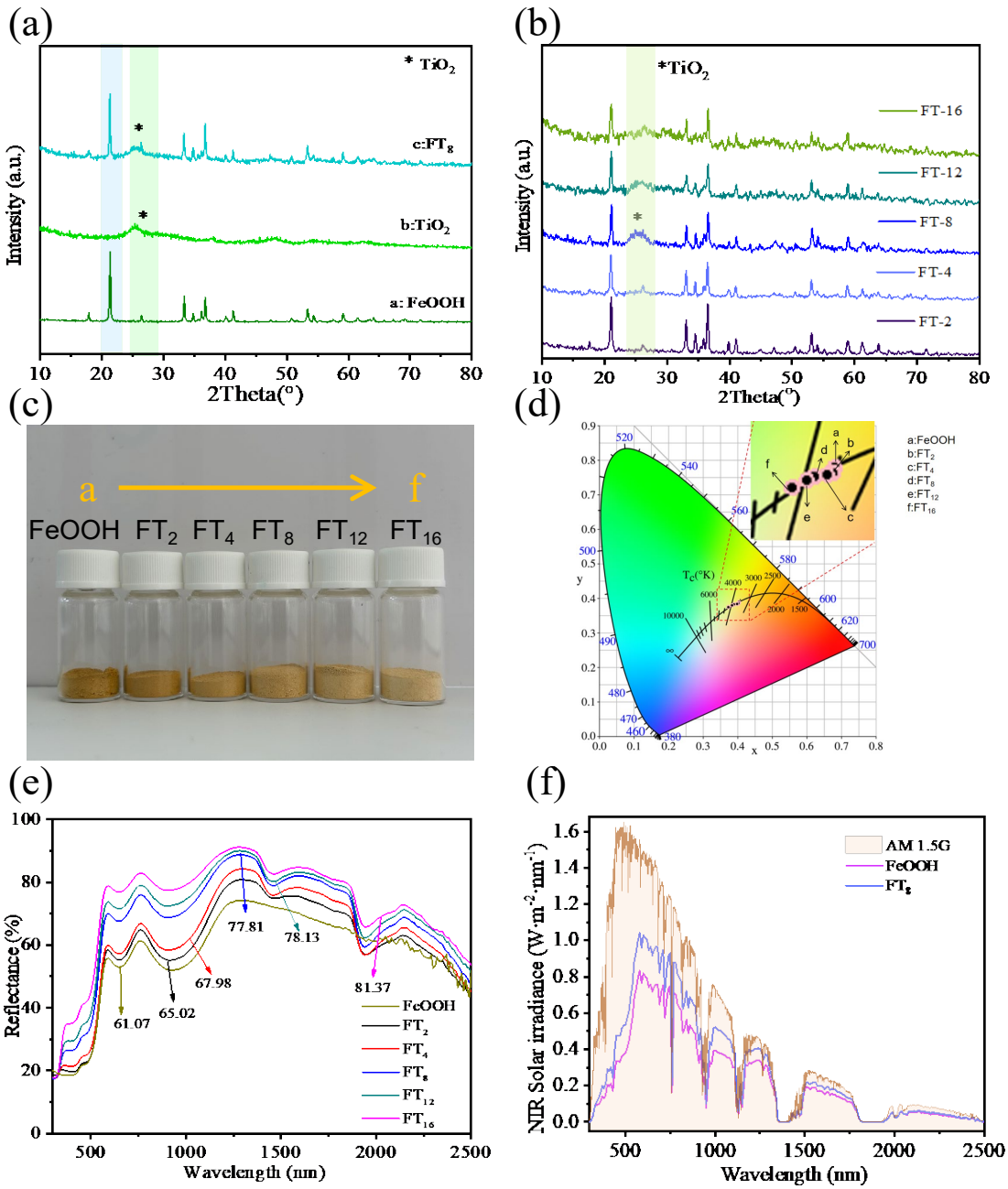

Fig. 3 XRD pattern (a, b), optical photos (c), CIE color coordinates (d), and reflection spectrum (e), and the solar reflectance energy distribution of coated pigments prepared under different TiO_2 dosages.

Table 2. Color difference parameters and reflectance of pigments under different TiO_2 dosages.

Samples	Quality percentage of TiO_2/%	*L**	*a**	*b**	TSR/%
FeOOH	0	70.33	12.91	33.87	49.3
TiO_2	100	98.47	0.27	2.17	90.6
FT_2	48.41	70.11	12.33	29.58	52
FT_4	65.23	75.01	11.65	30.21	54.3
FT_8	79.053	80.25	10.11	29.37	63.8
FT_{12}	84.923	82.03	9.14	28.11	65.6
FT_{16}	88.233	84.75	7.5	25.13	70.1

To better understand how the TiO_2 coating influences the optical properties of the pigment, we performed regression analysis between the TiO_2 content and color differences and reflectivity (Fig. 4a–e). The results indicate that the lightness value (*L**) increases with higher TiO_2 coating levels (Fig. 4a). The fitting equations are summarized in Table 3, showing a high correlation coefficient of 0.9922, which suggests a strong exponential relationship between TiO_2 coating and *L**, described by the equation $y = 0.15\times e^{-x/-19.08} + 69.62$. In contrast, the red-green (*a**) and yellow-blue (*b**) color parameters both decrease as the TiO_2 coating increases. Regression analysis reveals an exponential decline in both *a** and *b** values with increasing TiO_2 content, indicating a diminishing red-yellow hue in the pigment.

Regarding the reflectance properties, both TSR and NIR exhibit exponential growth with increasing TiO_2 coating (Fig. 4d and 4e). The high correlation coefficients in Table 3 confirm the strong relationship between TiO_2 content and reflectance.

Table 3. The fitting equations of *L**, *a**, *b** and reflectance of pigments with TiO_2 dosage.

	Equation	Parameters			
	$y = A_1\times e^{(-x/t1)} + y_0$	y_0	A_1	t_1	R^2
*L**	$y = 0.15\times e^{-x/-19.08} + 69.62$	69.62	0.15	-19.08	0.9922
*a**	$y = -5.87\times10^{-3}\times e^{-x/-13.06} + 12.69$	12.69	-5.87×10^{-3}	-13.06	0.99774
*b**	$y = -4.35\times10^{-5}\times e^{-x/-7.45} + 31.37$	31.37	-4.35×10^{-5}	-7.45	0.98430
TSR	$y = 0.1397\times e^{-x/-17.59} + 49.38$	49.38	0.1397	-17.59	0.99488
NIR	$y = 1.84\times e^{-x/-35.58} + 58.55$	58.55	1.84	-35.58	0.97871

Additionally, a linear correlation is observed between the *L** value and NIR (Fig. 4f), represented by the equation $y = 1.426x - 50.63$ with an R^2 value of 0.9895. As the pigment becomes lighter (higher *L**), the NIR of pigments also increases. In the CIE color space, the *L** value reflects the surface's visible light reflectivity (0 = black, 100 = white), while NIR indicates how well the material reflects near-infrared radiation (700–2500 nm) [18]. The linear relationship between *L** and NIR suggests that the scattering efficiency of pigment particles is consistent across both spectral ranges, implying similar effects of particle size and distribution on visible and near-infrared wavelengths. This consistency also reflects the pigment's uniform optical behavior and compositional stability.

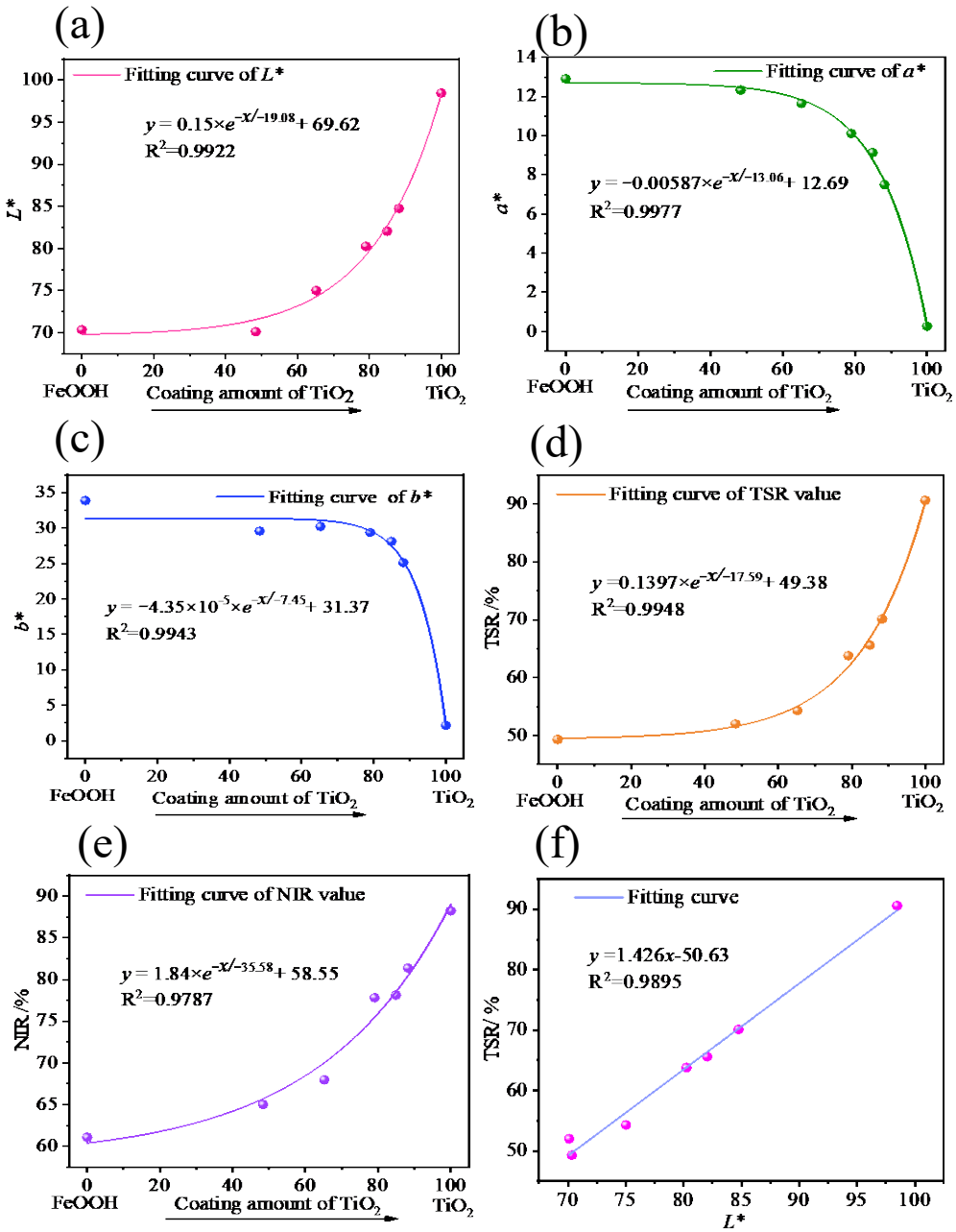

Fig. 4. The fitted curves of color difference parameters and reflectance of pigments with TiO_2 dosage (a-e), as well as the correlation between pigment brightness and total solar reflectance (f).

3.4 The influence of hydrolysis reaction solvent

In Fig. 5a, the XRD patterns of pigments prepared under different hydrolysis conditions exhibit nearly identical peak positions and intensities, maintaining the characteristic structure of FeOOH. These findings suggest that the hydrolysis solvent has minimal influence on the crystal structure of FeOOH, and even the smallest amount of water used is sufficient for the hydrolysis of butyl titanate.

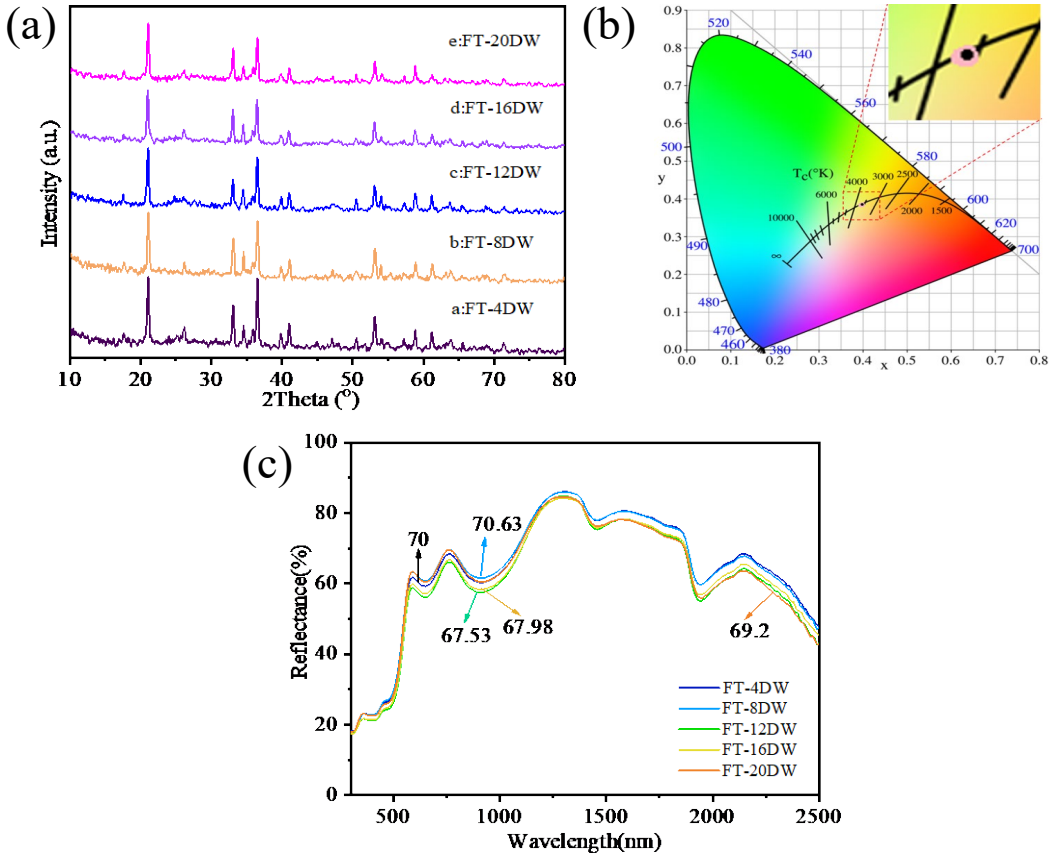

Fig. 5. The effects of hydrolysis solvent variations on the structural, color, and reflective properties of coated pigment, the XRD pattern (a), chromatic diagram (b) and near infrared reflectance (c) of coated pigment.

Fig.5b displays the chromaticity of pigments synthesized with varying water volumes in the CIE color space. The overlapping color coordinates and similar color difference values (Table 4) indicate that changes in water usage during the reaction have negligible effects on the color appearance of pigments。

The reflectance data under different water usage conditions are presented in Fig. 5c and Table 4. When 12 mL of water is used, the TSR is lowest at 53.7% and NIR at 67.53%. The highest TSR (57.1%) and NIR (70.63%) are achieved with 8 mL of water. The TSR values are the same when 4 mL and 20 mL of water are added, at 56.2%, and the NIR values are 70% and 69.2%, respectively. These results suggest that variations in water volume during the reaction do not significantly alter the degree of hydrolysis of butyl titanate or the resulting TiO_2 coating, leading to minimal changes of TSR and NIR values.

Table 4. Color difference parameters and reflectance of coated pigments under different water usage.

Samples	*L**	*a**	*b**	TSR/%	NIR/%
FT-4DW	75.71	11.49	29.84	56.2	70
FT-8DW	75.56	11.48	30.24	57.1	70.63
FT-12DW	74.6	11.83	30.07	53.7	67.53
FT-16DW	75.01	11.65	30.21	54.3	67.98
FT-20DW	74.91	11.85	30.36	56.2	69.2

3.5 Effect of reaction time

The XRD patterns in Fig. 6a show that the diffraction peaks remain consistent across different reaction time, preserving the FeOOH crystalline structure. This indicates that the selected hydrolysis times are sufficient for complete hydrolysis of butyl titanate and stable formation of the TiO_2 coating. In Fig. 6b and Table 5, the chromaticity of pigments synthesized under different reaction times overlaps significantly in the CIE color space, with minimal variation in color parameters. This suggests that reaction time has almost no effect on the hue of FeOOH, as all test time allow for adequate hydrolysis of the precursor.

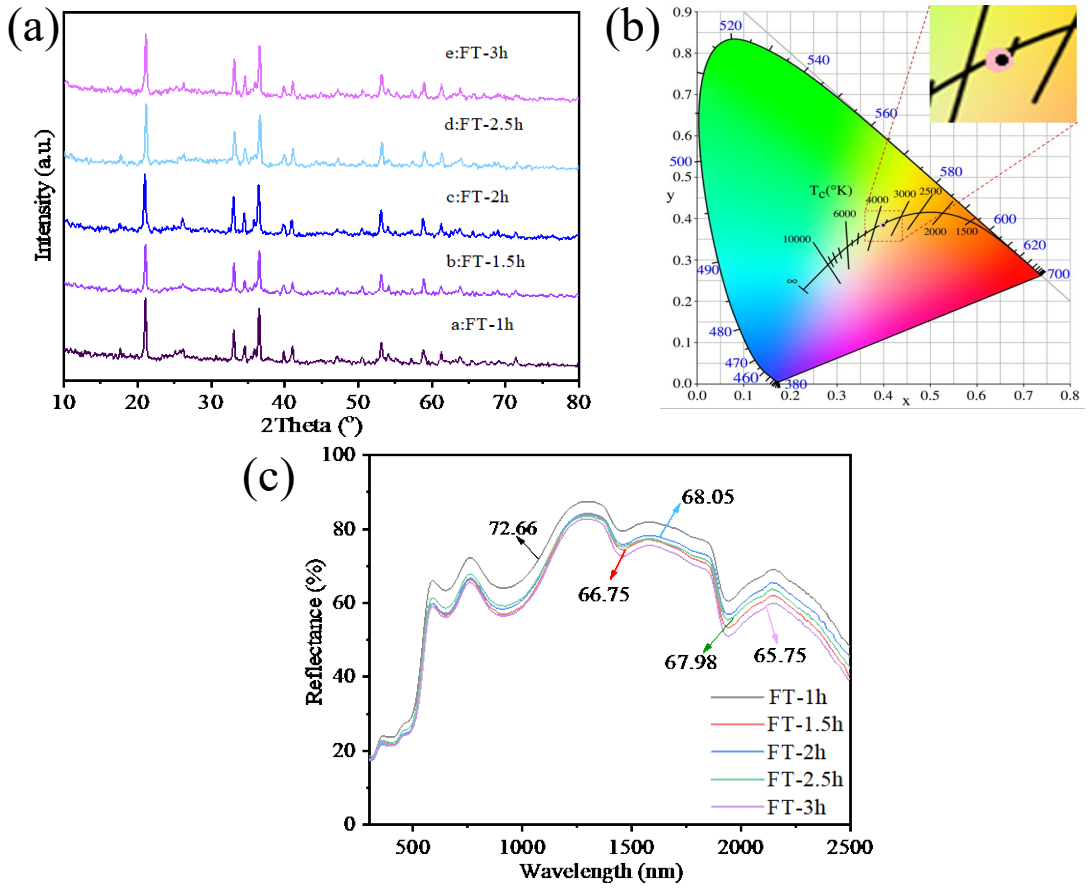

Fig. 6. The influence of reaction time on the structure, color, and reflectance of coated pigment, the XRD pattern (a), chromatic diagram (b) and near infrared reflectance (c) of coated pigment.

The reflectance performance under varying reaction times is shown in Fig.6c and Table 5. The lowest TSR (53%) and NIR (65.75%) are observed at a 3h reaction time (FT-3h), whereas the highest TSR (59%) and NIR (72.66%) are recorded at 1 h (FT-1h). The FT-2h shows the second-highest values (TSR: 55.1%, NIR: 68.05%). At 2.5 h, TSR is 54.3% and NIR is 67.98%, while at 1.5 h, TSR is 53.7% and NIR is 66.75%. These variations can be attributed to mechanical stirring during the preparation process, where prolonged reaction times could lead to partial detachment of the TiO_2 layer from the pigment surface, thereby reducing reflectance values.

Table 5. Color difference parameters and reflectance of coated pigment under different reaction times.

Samples	*L**	*a**	*b**	TSR/%
FT-1h	76.73	11.35	31.01	59
FT-1.5h	73.78	11.83	29.09	53.7
FT-2h	75.01	11.65	30.21	55.1
FT-2.5h	74.49	11.75	29.9	54.3
FT-3h	73.2	12.28	29.75	53

4. Conclusions

Yellow pigment FeOOH was successfully coated with TiO_2 by the sol-gel method to produce a coated pigment (FT*x*). The TiO_2 coating forms a compact layer of fine particles on the pigment surface, altering the original FeOOH morphology. TiO_2 remains in an amorphous state and does not interfere with the crystalline structure of the FeOOH. After coating, the pigment appears lighter in color, and its reflectivity increases with higher TiO_2 loading. The TSR of FT_{16} reaches 70.1%, with an NIR is 81.37%. The TiO_2 coating amount shows exponential correlations with both colorimetric parameters and reflectance, while a strong linear relationship exists between NIR and *L** value. The high reflectance of the coated pigment makes it a promising candidate for energy-efficient cooling applications as a “cool pigment”.

Availability of Data and Materials

Data will be made available on request.

Author Contributions

J. H. Lu, Q. Shen and M. H. Xu designed and performed the research study. J. R. Chu and X. Ling analyzed the data. J. H. Lu and M. H. Xu drafted the manuscript.

Acknowledgment

This work is supported by Huzhou Science and Technology Public Welfare Project (Research and Industrialization of Clay-based Green Energy-saving Composite Multi-functional Insulation and Heat Preservation Coatings for Building Use).

Funding

This project was supported by the Huzhou Science and Technology Public Welfare Project (Grant No.: 2025GG39).

Conflict of Interest

The authors declare no conflict of interest.

References

[1] S.P. Aswathy, C. V. Geethanjali, A. S. Kumar, V. S. Saji, S. M. A. Shibli, Surfaces and Interfaces **45**, 103882 (2024); https://doi.org/10.1016/j.surfin.2024.103882.
[2] D.F. Skripnuk, E. A. Samylovskaya, IOP Conference Series: Earth and Environmental Science **180**, 012021 (2018); https://doi.org/10.1088/1755-1315/180/1/012021.
[3] H. Zhang, J. Liu, F. Shi, T. Li, H. Zhang, D. Yang, Y. Li, Z. Tian, N. Zhou, Chemical Engineering Journal **431**, 133353 (2022); https://doi.org/10.1016/j.cej.2021.133353.
[4] P. K. Thejus, K.V. Krishnapriya, K. G. Nishanth, Solar Energy Materials and Solar Cells **219**, 110778 (2021); https://doi.org/10.1016/j.solmat.2020.110778.
[5] M. Xu, G. Pan, Y. Cao, Y. Guo, H. Chen, Y. Wang, Y. Wu, Surface and Interface Analysis **52**, 626-634 (2020); https://doi.org/10.1002/sia.6803.
[6] G. Zeng, J. Yang, R. Hong, Z. Li, Y. Chen, F. Li, Q. Wu, L. Liu, X. Jiang, Ceramics International **44**, 8788-8794 (2018); https://doi.org/10.1016/j.ceramint.2018.02.025.
[7] Q. Zheng, S. Xiong, X. Wu, J. Kuang, W. Liu, W. Cao, Materials **15**, 8310 (2022); https://doi.org/10.3390/ma15238310.
[8] L. Li, F. Luo, X. Yu, W. Xie, X. Sun, ACS Sustainable Chemistry & Engineering **9**, 16606-16616 (2021); https://doi.org/10.1021/acssuschemeng.1c05182.
[9] X. He, F. Wang, H. Liu, J. Li, L. Niu, Materials Letters **208**, 82-85 (2017); https://doi.org/10.1016/j.matlet.2017.05.047.
[10] J. Zou, P. Zhang, Ceramics International **46**, 3490-3497 (2020); https://doi.org/10.1016/j.ceramint.2019.10.063.
[11] J. Zou, Y. Chen, P. Zhang, Ceramics International **47**, 12661-12666 (2021); https://doi.org/10.1016/j.ceramint.2021.01.126.
[12] I. Arčon, A. Kodre, M. Mozetič, Vacuum **80**, 178-183 (2005); https://doi.org/10.1016/j.vacuum.2005.08.012.
[13] R. Snovski, J. Grinblat, M. T. Sougrati, J. C. Jumas, S. Margel, Journal of Magnetism and Magnetic Materials **349,** 35-44 (2013); https://doi.org/10.1016/j.jmmm.2013.08.043.
[14] M. Xu, G. Pan, Q. Shen, Y. Guo, M. Zhou, Q. Liang, Applied Surface Science **641**, 158525 (2023); https://doi.org/10.1016/j.apsusc.2023.158525.
[15] Z. Xing, J. Hu, M. Ma, H. Lin, Y. An, Z. Liu, Y. Zhang, J. Li, S. Yang, Journal of the American Chemical Society **141**, 19715-19727 (2019); https://doi.org/10.1021/jacs.9b08651.
[16] L. Wang, H. Tan, L. Zhang, B. Cheng, J. Yu, Chemical Engineering Journal **411**, 128501 (2021); https://doi.org/10.1016/j.cej.2021.128501.
[17] L. Wang, B. Cheng, L. Zhang, J. Yu, Small **17**, 2103447 (2021); https://doi.org/10.1002/smll.202103447.
[18] Z. J. Yu, J. B. Zhou, M. H. Xu , Y. F. Yang, Y. Y. Wang, Digest Journal of Nanomaterials and Biostructures **19**, 1719-1735 (2024); https://doi.org/10.15251/DJNB.2024.194.1719.